



Trans. Nonferrous Met. Soc. China 31(2021) 2909-2921

Transactions of Nonferrous Metals Society of China

www.tnmsc.cn



Strengthening of aluminium alloy 7005 through imposition of severe plastic deformation supplemented by different ageing treatments

R. BAKHSHI, M. H. FARSHIDI, S. A. SAJJADI

Department of Materials Science and Metallurgical Engineering, Ferdowsi University of Mashhad, Azadi Square, Mashhad, Iran

Received 9 September 2020; accepted 28 June 2021

Abstract: Strengthening of aluminium alloys 7xxx through the imposition of severe plastic deformation supplemented by ageing treatments is a challenge due to the limited workability of these alloys in cold deformation regimes. This study aims to comprehensively investigate the strengthening of aluminium alloy 7005 through the imposition of severe plastic deformation supplemented by two different ageing treatments: pre-deformation artificial ageing or post-deformation natural ageing. For this purpose, microstructure evolutions of the alloy processed through mentioned procedures were studied using X-ray diffraction and scanning electron microscopy while the alloy strengthening was evaluated using Vickers hardness measurement. Results show that a superlative strengthening is obtained through the imposition of severe plastic deformation supplemented by post-deformation natural ageing. For instance, the yield strength of the alloy increases to more than 400 MPa, about one-third greater than the counterpart amount after the usual T6 treatment. This superlative strength mainly occurs due to refinement of grains, an increase of dislocation density and an increase of volume fraction of the precipitates that appeared during natural ageing. Considering the applied models, it is inferred that the increase of volume fraction of precipitates that appeared during natural ageing has a determinative role in the strengthening of the alloy.

Key words: severe plastic deformation; strength; precipitation; ageing treatment; aluminum alloy 7005

1 Introduction

Aluminium alloys 7xxx (AA7xxxs) are known due to their attractive properties such as age-hardening capability, resistance to stress corrosion cracking and low density. These alloys containing Mg, Zn and probably Cu as their main alloying elements show the highest strength among all of the aluminium alloys. In AA7xxxs, the age-hardening usually occurs by the appearance of MgZn $_x$ precipitates through subsequent steps mentioned below:

Supersaturated solid solution (SSS)→

GP zones $\rightarrow \eta' \rightarrow \eta$

It has been shown that the GP zones appear at ageing temperatures of $20-120\,^{\circ}\text{C}$ and they are coherent with the aluminium lattice (SSS or α phase) bearing a mismatch of a few percents. Additionally, the η' precipitates appear at ageing temperatures of $120-250\,^{\circ}\text{C}$ and they have a hexagonal lattice characterized by a basal parameter (a) of 0.496 nm and an orthogonal parameter (c) of 1.402 nm. This hexagonal lattice is semi-coherent with the α phase whereas (0001) planes of the η' lay in parallel to (111) planes of the α phase by a mismatch of less than 1%. Comparatively, the η precipitates appear at ageing temperatures of $150-300\,^{\circ}\text{C}$ in a form of the hexagonal Laves lattice and they are incoherent with the α phase [1-6]. In addition to

crystallographic differences, the atomic proportion of Zn/Mg inside the mentioned precipitates is different and it gradually increases during the evolution of the GP zones to the η precipitates. As an illustration, this proportion is evaluated to be about 1 for the GP zones, 1.5 for the η' precipitates and 2 for the η precipitates [1,7]. Among aluminium alloys 7xxx, AA7005 is known for its attractive properties such as natural age-hardening capability and good weldability. Therefore, this alloy is used in the fabrication of multiple parts of different vehicles like bicycles and rapid trains. During the natural age hardening of a coarse-grained AA7005, an increase of the hardness is started after a few minutes of remaining at room temperature as a result of the formation of spheroidal GP zones. Successively, the Vickers hardness (VHN) of this material increases from about 50 to more than 80 at the end of one year of natural ageing [7,8]. Despite this attractive age hardening, the cold workability of the alloy becomes limited after a few days of natural ageing because of the occurrence of dynamic strain ageing (DSA) as a result of the appearance of GP zones [8].

During past decades, the imposition of severe plastic deformation (SPD) processes has been introduced as an excellent method for the strengthening of metals and alloys. Usually, this method is defined as the imposition of a plastic strain greater than 2, which causes a remarkable strain hardening, generally because of considerable grain refinement and an extensive increase of dislocations density [9,10]. While different aluminium alloys have been subjected to this method, the application of this method for aluminium alloys 7xxx has been a challenge due to their limited workability. As an illustration, the supplement of SPD to age hardening of AA7005 has been a challenge investigated by a couple of works [8,11-14]. While these works have proposed different procedures for this purpose, the following two procedures seem to be successful [8,12]: (1) the immediate imposition of SPD on the SSS (as-quenched alloy) supplemented by subsequent exposure of it to ageing; (2) the imposition of SPD on the artificially over-aged alloy which contains η' or η precipitates. Nonetheless, there is no comprehensive study that compares the effect of these two procedures on the strengthening of AA7005. Also, most of the previous studies on this

topic have qualitative approaches and they have failed to quantitatively evaluate different strengthening mechanisms arisen through the proposed procedures. Moreover, while most of the previous works have studied the artificial ageing of solid-solution treated AA7005 after the imposition of SPD, its natural-ageing after the imposition of SPD has remained less considered.

This work aims to comprehensively investigate the effect of SPD supplemented by pre/postdeformation ageing treatments on the strength of AA7005. For this purpose, the alloy is subjected to two different heat treatments and afterwards, it is rolled at the ambient temperature until the imposition of an equal strain of about 3. After rolling, the alloy is kept at room temperature for up to 24 months to pursue its natural ageing. During this period, the hardening of the alloy is evaluated using VHN measurements while its microstructure evolutions are observed by scanning electron microscopy (SEM) and X-ray diffraction (XRD). Finally, the results of these experiments are compared with a few of the generally accepted strengthening models to obtain a better insight into the strengthening effect of SPD supplemented by age-hardening treatments.

2 Experimental

The aluminium alloy is received in form of a warm-rolled slab halving a thickness of 15 mm. Table 1 lists the chemical composition of the received slab evaluated using spark emission spectroscopy. As can be seen in Table 1, the evaluated chemical composition of the received slab is very close to that of the AA7005. The received slab was cut into different pieces and then, two different types of specimens were prepared by planning the different heat treatments before SPD as follows.

- (1) Solid solution treated and rolled (SSR): Solution treated at 753 K for 1.5 h, quickly quenched in water and then immediately subjected to the SPD.
- (2) Aged and rolled (AGR): Solution treated at 753 K for 1.5 h, quickly quenched in water, artificially aged at 473 K for 2 h and then subjected to the SPD.

It has been reported that the mentioned solution treatment causes the formation of

supersaturated alloy through the dissolution of MgZn_x precipitates while the mentioned artificial ageing results in the wide-spread formation of η' precipitates inside the alloy [11-14]. SPD processing of the alloy is accomplished through rolling at room temperature. During rolling, when the thicknesses of AGR and SSR specimens reached 15, 3 and 0.8 mm, different pieces were separated from them to pursue metallurgical studies mentioned below. Hereafter, AGR_v and SSR_v refer to two different specimens cold rolled to a thickness of ymm through AGR and SSR procedures, respectively. The tolerance of the thickness of specimens was $\pm 10\%$ of their nominal thickness. Notably, the equivalent plastic strains imposed by cold rolling on specimens with thicknesses of 15, 3 and 0.8 mm are equal to 0, 1.8 and 3.4, respectively. It is noteworthy that the received slab was subjected to a plastic strain of about 3 during its previous warm rolling.

Different AGR and SSR specimens were kept at room temperature for up to 24 months after cold rolling. During this period, the VHN of specimens were measured using an indentation load of 4.9 N. Also, tensile tests were achieved on SSR0.8 and AGR0.8 specimens after 24 months of remaining at room temperature using a strain rate of 2×10^{-3} s⁻¹. After 0.25, 5 and 24 months of remaining at room temperature, XRD characterization of each specimen was accomplished by the Unisantis-XMD300 and D8-Bruker machine using Cu K_a X-ray over a range of diffraction angle (2θ) from 20° to 90° by a step size of 0.01°. Considering the results of XRD, Williamson-Hall (WH) method was applied for the estimation of the dislocation density of specimens while the Debye-Scherer (DS) method was applied for the calculation of the average radius of the precipitates. Details of the WH and the DS methods were presented in previous works [15–18].

Observations of the microstructure of specimens were accomplished by the TESCAN MIRA3-XMU FESEM machine using different magnifications in a range of 5000–75000. During FESEM studies, the chemical composition of precipitates was measured using energy-dispersive X-ray spectroscopy (EDXS). Also, MIP5 software was applied for the evaluation of precipitates fractions through analyzing SEM images. Moreover, the electron backscattering diffraction (EBSD)

observations of the microstructure of specimens were accomplished by JSM-7001F EBSD equipped with SEM machine under an acceleration voltage of 15 kV. INCA 4.09 software was applied to analyzing the results of EBSD observations. More details about the method of EBSD observations were presented elsewhere [19].

Table 1 Evaluated chemical composition of received slab (wt.%)

Cr	Cu	Zr	Fe	Mg	Mn	Si	Ti	Zn	Al
0.2	0.07	0.1	0.29	1.2	0.08	0.11	0.03	4.72	Bal.

3 Results

3.1 Effect of applied treatment on evolution of microstructure

Figure 1 shows the XRD patterns of AGR and SSR specimens which are remained at room temperature for 8 d after rolling. As can be seen here, different peaks related to MgZn_x precipitates are present in the XRD patterns which illustrate the existence of these precipitates inside these specimens. Considering the applied heat treatments and the ageing behaviour of AA7005 mentioned above, one may infer that the mentioned peaks inside XRD patterns of AGR specimens are related to η' precipitates formed during artificial predeformation ageing. Also, regarding the above mentioned explanations about the natural ageing behaviour of the alloy, MgZn_x related peaks inside XRD patterns of SSR specimens can be associated with the GP zones formed during the postdeformation natural ageing. Also, the broadening of XRD peaks related to aluminium (α phase) by the increase of rolling strain can be seen in Fig. 1. Similar results have been seen inside XRD profiles of both types of specimens subjected to longer remaining time at room temperature.

Figure 2 compares variations of the average radius of $MgZn_x$ precipitates of different specimens during the period of remaining at room temperature. As can be seen from Fig. 2, precipitates of SSR specimens show considerable growth during the period of remaining at room temperature attributed to the decomposition of solid solution. It is also notable that the precipitates of SSR specimens are coarser than those observed during the natural ageing of unstrained AA7xxx alloys. As an illustration, it is reported that the radius of GP zones

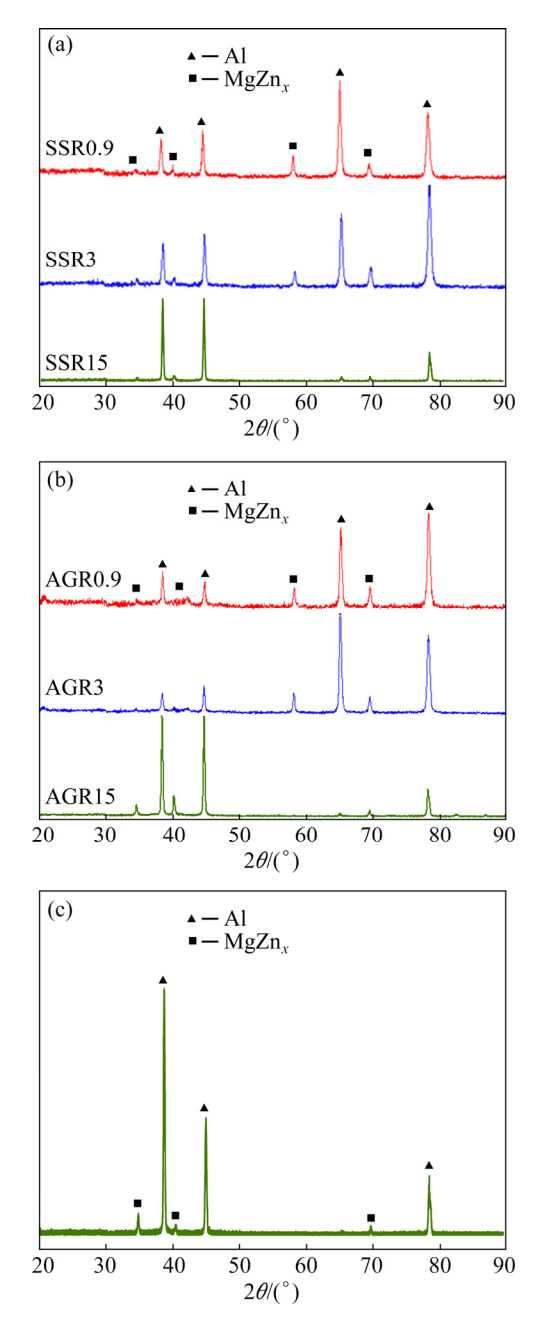


Fig. 1 XRD patterns of SSR (a) and AGR (b) specimens remaining at room temperature for 8 d, and XRD pattern of as-received specimen (c)

appeared during the natural ageing of unstrained coarse-grained AA7xxx alloys is in order of a few nanometers [5,6,20,21]. Correspondingly, the appearance of coarser precipitates during ageing of severely strained supersaturated aluminium alloys has been previously reported and it is attributed to the extensive increase of diffusion rate as a result of grain refinement and increase of dislocation density [22–24]. Similar to what seen for SSR specimens, the evaluated average radius of precipitates of AGR specimens is remarkably coarser

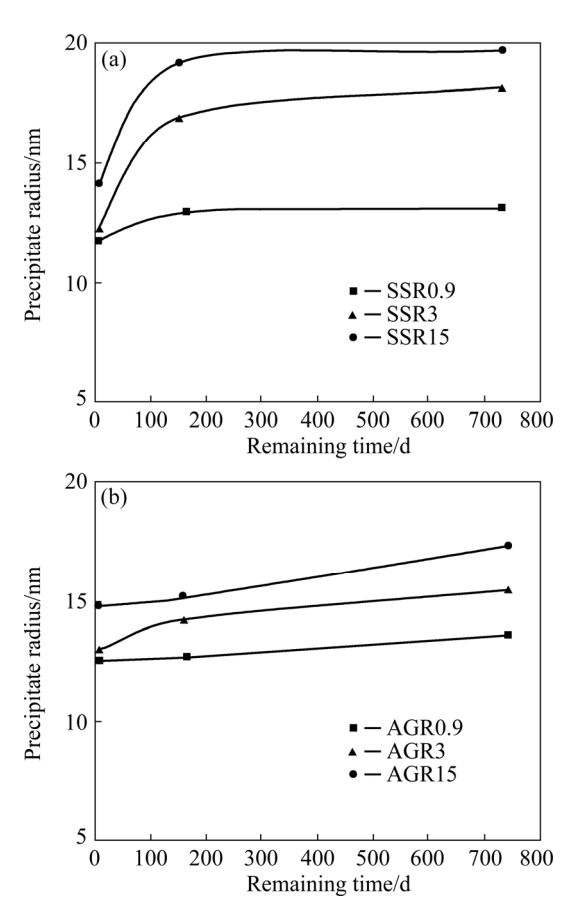


Fig. 2 Variation of average radius of precipitates of SSR (a) and AGR (b) specimens remaining at room temperature for different time

than 5 nm reported for the radius of η' precipitates appeared during similar artificial ageing of Al-Mg-Zn alloys [12,14]. This unstrained phenomenon can be clearly explained by the formation of precipitates of AGR specimens during artificial pre-deformation ageing of a warmly rolled received slab that has relatively fine grains as discussed below. It is also notable that the average radius of precipitates of both types of specimens decreases by the increase of rolling strain. For SSR specimens, this effect could be explained by the appearance of more nucleation sites of precipitation since the area of grain boundaries and the dislocations pile-ups are increased by rolling [9,10]. On the other hand, the decrease of radius of precipitates inside AGR specimens through rolling can be attributed to a limited dissolution of η' precipitates inside aluminium (α phase) as a result of the imposition of SPD according to the previous works [12,25].

Figure 3 shows the variations of dislocation densities of different specimens during the period of

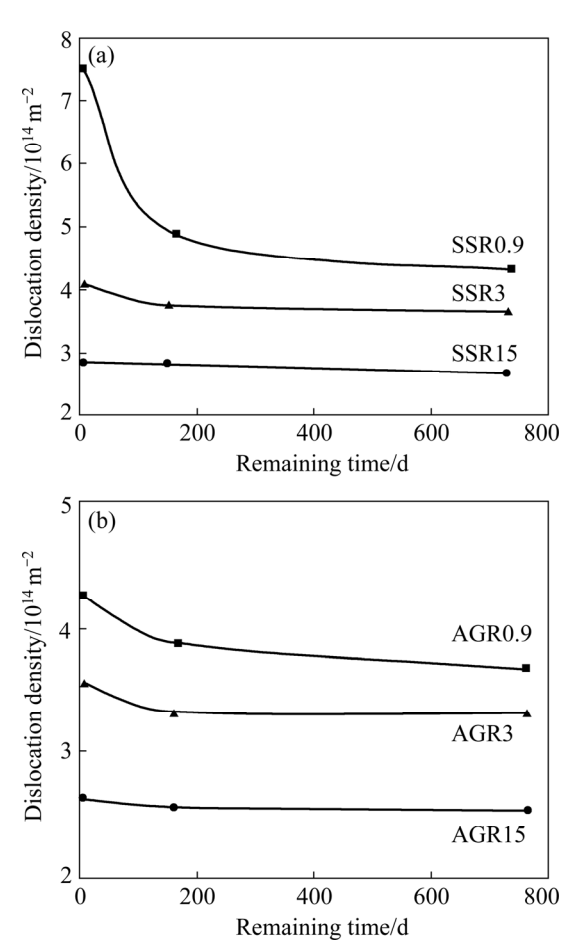


Fig. 3 Variation of dislocation densities of SSR (a) and AGR (b) specimens remaining at room temperature

remaining at room temperature. As can be seen, dislocation densities of different specimens after imposition of SPD range from 3×10^{14} to 8×10^{14} m⁻². These results are comparable with those of previous works which have reported the dislocation density of SPDed AA7xxx in a range of $3\times10^{14}-5\times10^{14} \text{ m}^{-2}$ [13,15]. It is also notable that the dislocation densities of different specimens decrease during the period of remaining at room temperature. This decrease of dislocation density happens because of the occurrence of dislocations annihilation inside aluminium even at ambient temperature as a result of high mobility of dislocations of this metal [26,27]. Also, comparison of Figs. 3(a) and (b), it is clear that the dislocation densities of AGR specimens are remarkably lower versus the SSR counterparts. This phenomenon is interpreted as a higher susceptibility for dislocation multiplication inside SSR specimens in comparison to what is seen inside AGR specimens. During SPD of SSR specimens, the alloying elements like Mg and Zn mainly remained

in the solute form inside aluminium (α phase). Despite this, the alloying elements of AGR specimens mainly precipitated before SPD which indicates depletion of α phase of AGR specimens from these elements. Considering that dislocation multiplication is mainly activated the Frank-Read dislocation sources through performed by anchored dislocations [28], one may infer that the anchoring effect of solute atoms on dislocations is more effective in comparison to a similar effect of precipitates. This phenomenon could be explained by the more overall anchoring effect of solute atoms in comparison to the local anchoring effect of precipitates. Notably, the solute atoms can play their anchoring effect through the formation of a solute atmosphere around edge dislocations and/or segregation on stacking faults (SF) between Shockley partial dislocations [29–31]. Since the sizes of these solute atmospheres and/or SF are remarkably finer in comparison to those of precipitates, one can infer that the anchoring effect of solute atoms is more overall in comparison to a similar effect of precipitates.

Figures 4-6 compare microstructures of different specimens observed by FESEM. Table 2 compares the volume fractions of precipitates of different specimens evaluated by the analysis of Figs. 4 and 5. As shown in Table 2, the volume fractions of precipitates of different specimens vary in a range of a few percents. Correspondingly, previous works have reported the volume fraction of precipitates of similar Al-Mg-Zn alloys subjected to different thermomechanical treatments in a range of 1%-13.4% [12,32,33]. As can be seen in Table 2, the volume fractions of precipitates of SSR specimens considerably increase with the increase of remaining time at room temperature. This result indicates the progression of natural ageing of these specimens. In comparison, the volume fractions of precipitates of AGR specimens are almost constant during the period of remaining at room temperature. This result can be attributed to a near-complete depletion of the alloying elements from the α phase during pre-deformation artificial ageing of AGR specimens. A limited increase of volume fractions of precipitates of AGR specimens during the period of remaining at room temperature could be explained by re-precipitation of solute atoms dissolved during SPD and/or precipitation of the solute atoms remained in the α phase after

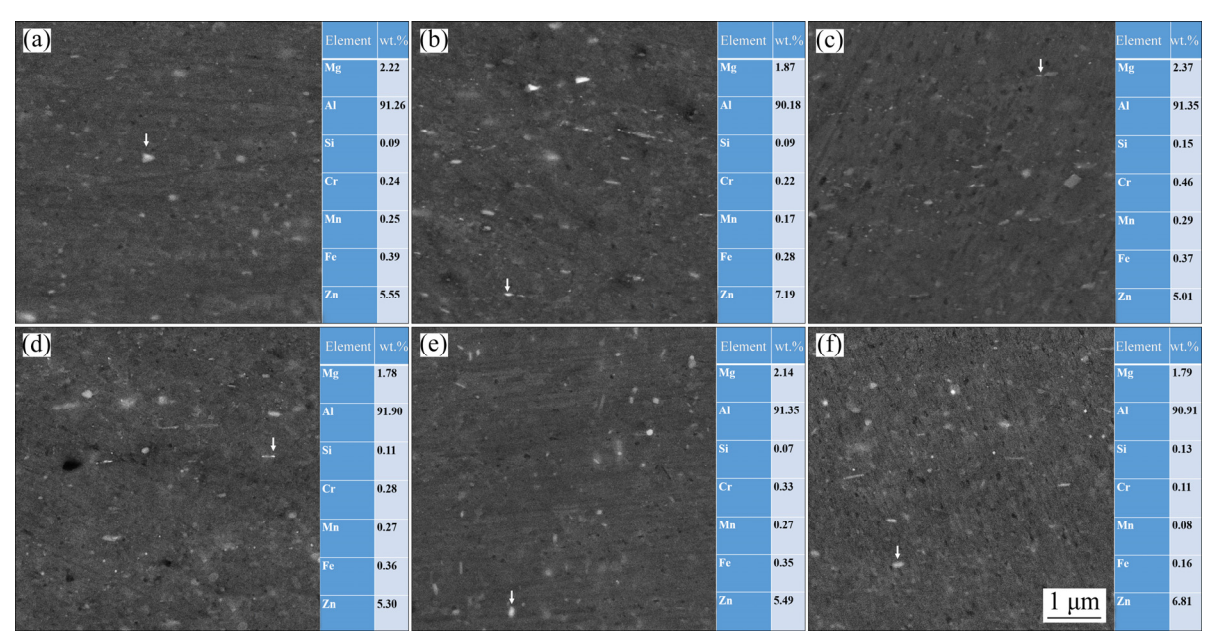


Fig. 4 Microstructures of SSR specimens observed by SEM: (a, b) SSR0.8; (c, d) SSR3; (e, f) SSR15 ((a, c, e) are obtained after 5 months, and (b, d, f) are obtained after 24 months. EDXS chemical compositions of the precipitates indicated by white arrows are presented in related tables)

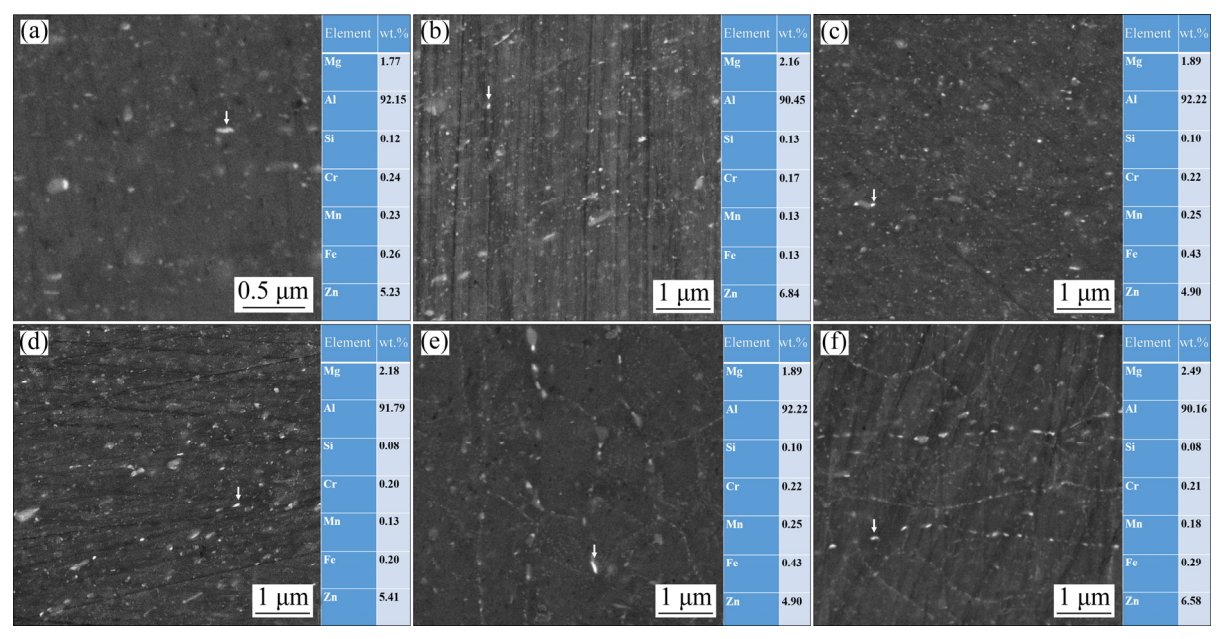


Fig. 5 Microstructures of AGR specimens observed by SEM: (a, b) AGR0.8; (c, d) AGR3; (e, f) AGR15 ((a, c, e) are obtained after 5 months, and (b, d, f) are obtained after 24 months. EDXS chemical compositions of the precipitates indicated by white arrows are presented in related tables)

pre-deformation artificial ageing. As shown in Figs. 4 and 5, the sizes of precipitates of both types of specimens are in order of tens of nanometers. These results are in agreement with the above-mentioned XRD results about the presence of the $MgZn_x$ precipitates inside different specimens. Also, one may see that precipitates of the SSR specimens mainly have spheroidal shapes attributed to the GP

zones. In comparison, precipitates of the AGR specimens mainly have elliptical shapes attributed to the η' precipitates [1–3,12]. It is also notable that relatively coarse AlFeSi particles are observed in the microstructures of specimens similar to that shown in Fig. 6. These particles were probably formed during the casting of the alloy as a result of the presence of iron and silicon in the alloy. Since

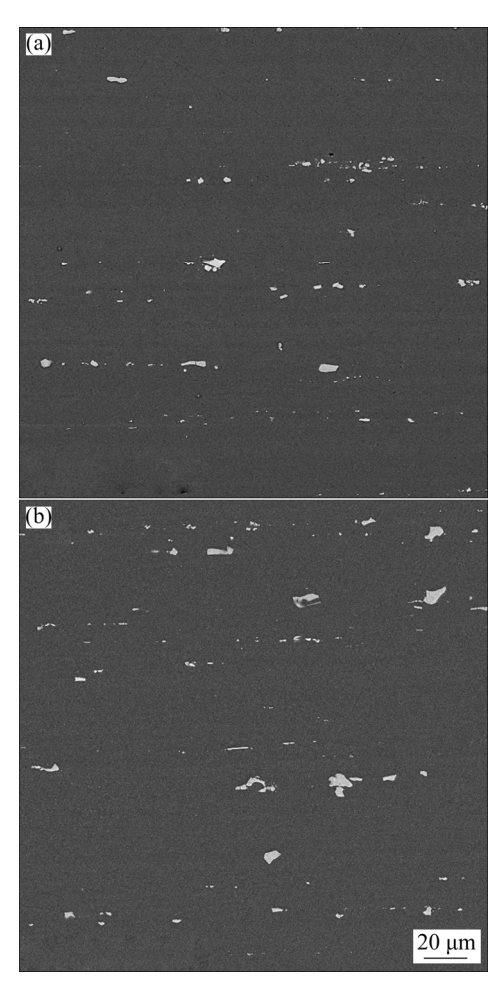


Fig. 6 Microstructures of SSR15 (a) and AGR15 (b) specimens showing the presence of AlFeSi particles

Table 2 Volume fraction of precipitates of specimens remaining at room temperature for different time

C	Precipitate content/vol.%				
Specimen -	After 5 months	After 24 months			
SSR15	2.4	3.9			
SSR3	2.3	3.7			
SSR0.8	2.1	3.5			
AGR15	6.6	6.9			
AGR3	6.5	6.9			
AGR0.8	6.1	6.8			

the solution of these particles in the α phase is negligible, they have an insignificant role in the heat treatment of the alloy. However, they could be fragmented into smaller particles due to the imposition of SPD as reported in Refs. [34,35].

Figures 7(a-f) compare the microstructures of different specimens observed by SEM-EBSD. The

colour of each grain represents its pole regarding the inverse pole figure triangle presented in Fig. 7(g) and therefore, neighbour grains can be characterized from each other. As can be seen in Figs. 7(a) and (b), the microstructure of the alloy after initial solution treatment consists of grains elongated toward the rolling direction. This microstructure was developed during the initial warm rolling of the received slab due to the absence of dynamic recrystallization. Delayed occurrence of static recrystallization in AA7xxx alloys is a well-known phenomenon attributed to the pinning effect of insoluble dispersoids at grain boundaries and it is usually called the Zener effect. Usually, dispersoids pinning are intermetallic compounds of aluminium with Sc, Zr, Mn and Cr elements [36,37]. As shown in Figs. 7(c) and (e), while the elongated grains are still present in the microstructures of AGR3 and SSR3 specimens, a partial formation of relatively equiaxed grains in these specimens is noticeable. Formation of the equiaxed grains occurs through fragmentation of the initially elongated grains through the incidence of micro-shear bands and cell bands. This phenomenon, usually called continuous dynamic recrystallization (CDRX), occurs during the imposition of SPD on metals and alloys even at clod regimes [9,10]. As shown in Figs. 7(d) and (f), the microstructures of AGR0.8 and SSR0.8 specimens are almost occupied by the equiaxed grains, indicating that the CDRX has impressively progressed in both specimens. Table 3 compares the grain size of different specimens evaluated by SEM-EBSD observations. As can be seen here, a remarkable grain refinement occurred through the imposition of SPD on both types of specimens. For instance, the grain size of the alloy decreases from about 12 µm before the SPD to about 1 µm after the imposition of a plastic strain of about 3. Also, it is notable that the degree of grain refinement versus the amount of plastic strain inside both types of specimens is similar. This result demonstrates a negligible effect of the pre-deformation heat treatments on the grain refinement of the alloy through the imposition of SPD.

3.2 Variation of mechanical properties through applied treatments

Figure 8 compares variations of the Vickers hardness of different specimens during the period of

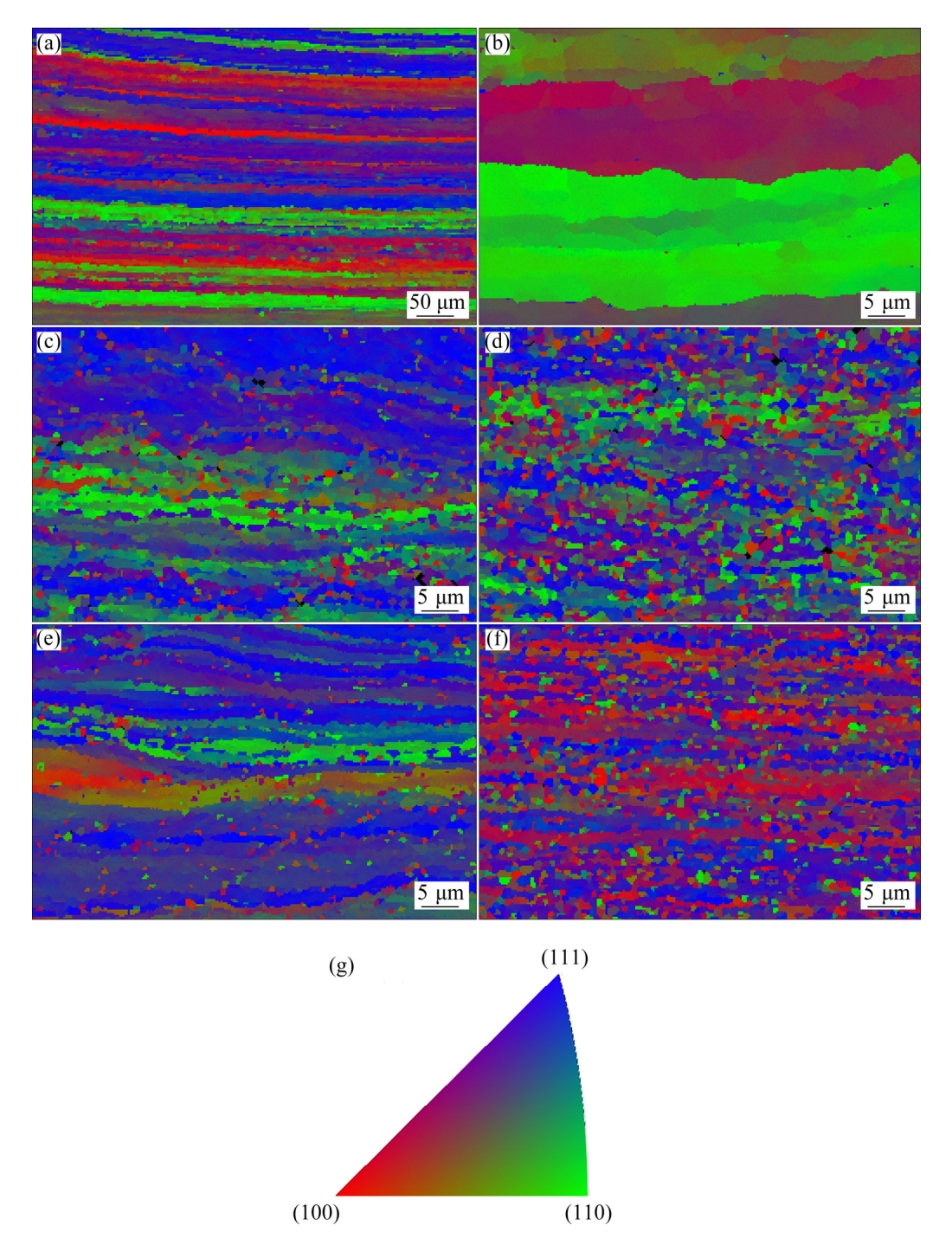


Fig. 7 Microstructures of different specimens observed by SEM-EBSD: (a, b) 15 mm-thick slab after solution treatment in different magnifications; (c) SSR3; (d) SSR0.8; (e) AGR3; (f) AGR0.8; (g) Inverse pole figure triangle

Table 3 Average grain size of different specimens

	1		
Specimen	Average grain size/μm		
Received slab after solution	12±5		
treatment			
AGR3	1.8 ± 0.4		
SSR3	1.5±0.3		
SSR0.8	1.1±0.3		
AGR0.8	1.1 ± 0.2		

remaining at room temperature. As can be seen here, the SSR specimens show greater hardness in comparison with their AGR counterparts. The observation of this phenomenon immediate after rolling could be attributed to the higher dislocation densities of SSR specimens. However, the differences in the hardness of both types of specimens increase during the period of remaining

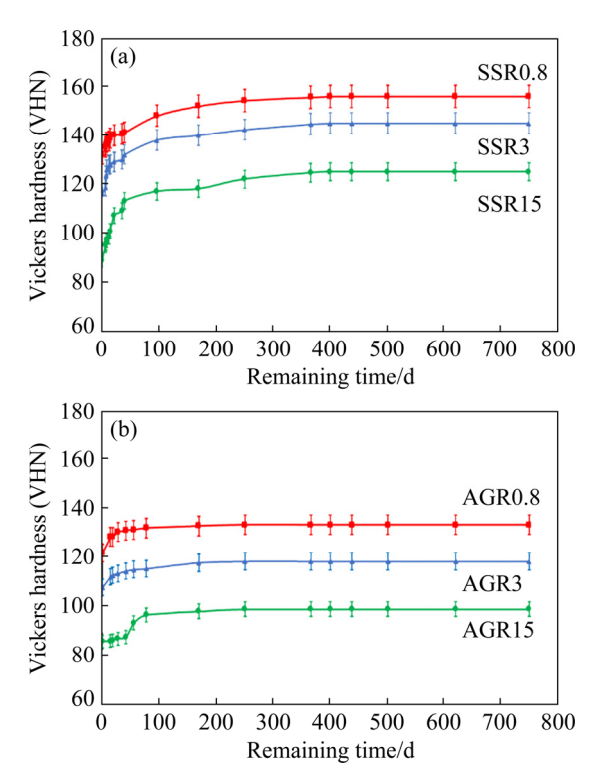


Fig. 8 Variation of VHN of SSR (a) and AGR (b) specimens during period of remaining at room temperature

at room temperature in opposition to variations of their dislocation densities shown in Fig. 3. Considering different heat treatments of two types of specimens before rolling, the increase of difference of their hardness can be attributed to the strengthening effect of GP zones that appeared through the natural ageing of SSR specimens [5-7,20,21]. It is also notable that the increase of hardness of SSR15, SSR3 and SSR0.8 during 24 months of natural ageing is equal to 36.5, 29 and 24 VHN, respectively. Considering similar natural ageing behaviours of these specimens, one may relate the smaller increase of hardness through natural ageing of SSR3 and SSR0.8 to a considerable decrease of their dislocation densities during the natural ageing period shown in Fig. 3. In contrast to SSR specimens, the hardness of AGR specimens shows a slight increase during the first few months of natural ageing which could be related to the limited formation of GP zones from solute atoms of the α phase. After this slight increase, the hardness of AGR specimens remains almost constant, which indicates the relative stability of their microstructures in agreement with that presented in Fig. 3, Fig. 5 and Table 2.

Figure 9 compares the results of tensile tests of AGR0.8 and SSR0.8 after 24 months of remaining at room temperature. As can be seen here, the SSR0.8 shows a greater strength in comparison with the AGR0.8. This result is in agreement with the results of the VHN measurement shown in Fig. 8. It is also notable that the fracture strain of the SSR0.8 is lower in comparison to that for the AGR0.8. This phenomenon can be related to the occurrence of DSA as a result of the appearance of GP zones during the natural ageing of SSR0.8 as discussed above [8]. Also, one can see that the yield strength of the SSR0.8 specimen is one-third greater than that of the AA7005 subjected to the usual T6 treatment.

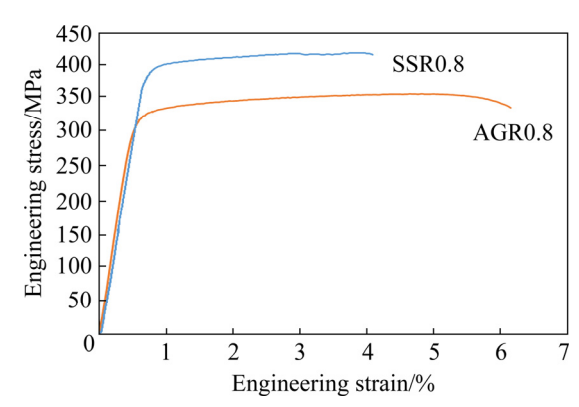


Fig. 9 Result of tensile test for AGR0.8 and SSR0.8 after 24 months of remaining at room temperature

4 Discussion

Considering the above-mentioned results, one may investigate the correlation of microstructure evolution of the alloy and its strengthening through the applied treatments. For this purpose, four different strengthening mechanisms involved during the mentioned treatments should be considered: the refinement of grains, the increase of dislocation density, the solid solution and the precipitation. The strengthening effect of grain refinement ($\Delta \sigma_{\rm GB}$) can be measured using the Hall–Petch equation presented as

$$\Delta \sigma_{\rm GB} = KD^{-1/2} \tag{1}$$

where D is the grain size of the alloy, and K is a constant evaluated as 0.083 for AA7005 [38]. Also, the strengthening effect of the increase of dislocation density ($\Delta\sigma_{\rm Disl}$) is measured as follows:

$$\Delta \sigma_{\text{Disl}} = M\alpha G b \rho^{1/2} \tag{2}$$

where ρ is the dislocation density, M is Tailor factor evaluated as 2.7 for rolled AA7xxx alloys, α is a constant of about 0.25, G is the shear module of aluminium considered as 26 GPa, and b is the Burgers vector magnitude of aluminium equal to 0.28 nm [12,13,15]. Also, the solid solution strengthening ($\Delta \sigma_{\rm SS}$) can be evaluated as follows [12]:

$$\Delta\sigma_{\rm SS} = M(20.5C_{\rm Mg}^{2/3} + 3.1C_{\rm Zn}^{2/3}) \tag{3}$$

where C_{Mg} and C_{Zn} are concentrations of Mg and Zn elements in mass fraction.

As shown by GLADMAN [39], when dislocations traverse precipitates by cutting, the coherency strengthening of precipitates ($\Delta \sigma_{\text{Coh}}$) can be evaluated by one of the following equations:

$$\Delta \sigma_{\rm Coh} = 4.1 MG \delta^{3/2} \left(\frac{rf}{b} \right)^{1/2} \tag{4}$$

$$\Delta \sigma_{\text{Coh}} = 0.7 MG \delta^{1/4} f^{1/2} \left(\frac{b}{r}\right)^{3/4}$$
 (5)

where δ is the relative mismatch between the dislocation glide plane of α phase and its counterpart inside precipitates, r is the precipitate radius, and f is the volume fraction of precipitates. GLADMAN [39] demonstrated that Eq. (4) should be applied for fine precipitates while Eq. (5) is proper for coarser precipitates. A critical precipitate radius (r^*) for the transition of its coherency strengthening from Eq. (4) to Eq. (5) can be calculated as follows:

$$r^* = \frac{b}{4\delta} \tag{6}$$

On the other hand, considering the mole ratio of Zn/Mg equal to 1 for GP zones and regarding the metallic radii of Al, Mg and Zn equal to 0.142, 0.160 and 0.134 nm, the mismatch of GP zones with α phase is evaluated as 0.035. Also, the mismatch of (0001) plane of the η' with (111) plane of the α phase has been reported as 0.003 [3]. Regarding these numbers, the r^* values of GP zones and η' would be calculated as 2.0 and 23.3 nm, respectively. Therefore, considering the average radius of precipitates of SSR specimens evaluated by the DS method and supposing that these precipitates are GP zones, one can infer that Eq. (5) is suitable for the calculation of the coherency strengthening of SSR specimens.

Similarly, supposing precipitates of the AGR specimens as η' and regarding their average radius evaluated by the DS method, it can be inferred that Eq. (4) is proper for calculation of the coherency strengthening of AGR specimens. On the other hand, when dislocations bypass precipitates through the Orowan mechanism, the strengthening effect of precipitates can be calculated as follows [13]

$$\Delta \sigma_{\rm BP} = \frac{0.85MGb}{2\pi(L - 2r)} \ln\left(\frac{2r}{b}\right) \tag{7}$$

where L is the average distance between precipitates calculated as follows [40]:

$$L = \sqrt[3]{\frac{4\pi}{3f}}r\tag{8}$$

Combining Eqs. (4)–(7), the precipitation strengthening ($\Delta \sigma_{Pr}$) of the alloy can be evaluated as

$$\Delta \sigma_{\text{Pr}} = \text{Min} \{ \Delta \sigma_{\text{Coh}}, \ \Delta \sigma_{\text{BP}} \}$$
 (9)

Considering what mentioned above, Eqs. (1)–(9) can be applied to measuring a hypothetical strength (σ_{YI}^{Hyp}) for each specimen regarding its observed microstructural characteristics as follows:

$$\sigma_{\rm Yl}^{\rm Hyp} = \sigma_0 + \Delta \sigma_{\rm GB} + \Delta \sigma_{\rm Disl} + \Delta \sigma_{\rm SS} + \Delta \sigma_{\rm Pr} \tag{10}$$

where σ_0 is the frictional strength of aluminium lattice considered as 1 MPa [41]. On the other hand, an equation has been proposed to estimate the yield strength of aluminium alloys 7xxx regarding their Vickers hardness (VHN, H_V) as follows [42]:

$$\sigma_{\rm Yl}^{\rm Es} = 0.383 H_{\rm V} - 182.3 \tag{11}$$

Considering Eq. (11) and the measured hardness of specimens shown in Fig. 8, the yield strengths of AGR0.8 and SSR0.8 specimens after 24 months of remaining at room temperature are evaluated about 327 and 415 MPa, respectively. These results are very close to those of tensile tests of the specimens shown in Fig. 9. Therefore, one can use Eq. (11) to compare the experimentally estimated yield strength of a specimen (σ_{YI}^{Es}) with its hypothetical yield strength (σ_{YI}^{Hyp}).

Tables 4 and 5 compare the hypothetical yield strengths of specimens with their experimentally estimated yield strength. As can be seen in Tables 4 and 5, there is a general agreement between the hypothetical strength of specimens on one side and their experimentally estimated yield strength on another side. This general agreement can verify the

Table 4 Comparison of σ_{VI}^{Hyp} and σ_{VI}^{Es} of SSR specimens after different remaining time at room temperature

Specimen	Remaining time/month	$\Delta\sigma_{ m Disl}/ m MPa$	$\Delta\sigma_{\mathrm{GB}}/\mathrm{MPa}$	$\Delta\sigma_{\mathrm{Pr}}/\mathrm{MPa}$	$\Delta\sigma_{ m SS}/{ m MPa}$	$\sigma_{ m Yl}^{ m Hyp}$ /MPa	$\sigma_{ m Yl}^{ m Es}$ /MPa
SSR15	0	83	24	0	86	194	157
SSR15	5	83	24	139	47	294	270
SSR15	24	80	24	173	8	286	296
SSR3	0	99	68	0	86	254	262
SSR3	5	95	68	149	49	362	354
SSR3	24	94	68	179	16	358	373
SSR0.8	0	136	79	0	86	302	323
SSR0.8	5	109	79	174	53	416	400
SSR0.8	24	102	79	225	22	429	415

Table 5 Comparison of $\sigma_{v_1}^{Hyp}$ and $\sigma_{v_1}^{Es}$ of AGR specimens after different remaining time at room temperature

Specimen	Remaining time/month	$\Delta\sigma_{ m Disl}/ m MPa$	$\Delta\sigma_{ m GB}/{ m MPa}$	$\Delta\sigma_{\mathrm{Pr}}/\mathrm{MPa}$	$\Delta\sigma_{ m SS}$ /MPa	$\sigma_{ m Yl}^{ m Hyp}$ /MPa	$\sigma_{ m Yl}^{ m Es}$ /MPa
AGR15	5	79	24	89	26	219	195
AGR15	24	79	24	98	22	224	192
AGR3	5	90	62	86	27	266	268
AGR3	24	90	62	92	22	267	267
AGR0.8	5	97	79	78	32	287	325
AGR0.8	24	94	79	84	23	281	327

applied method to associate the yield strengths of the specimens with their microstructural characteristics. Comparing Tables 2, 4 and 5, one can see that although the volume fraction of precipitates inside naturally aged SSR specimens is lower in comparison to that in AGR specimens, the precipitation strengthening of naturally aged SSR specimens is considerably greater than that of AGR specimens. Similarly, it has been reported that the natural ageing of the SPD processed Al-4Zn-2Mg alloy causes a greater strengthening effect in comparison to a similar effect caused by its artificial ageing. This phenomenon is despite what is seen for the unstrained Al-4Zn-2Mg alloys which show more strength through the formation of η' during artificial ageing [14]. The enhanced strength of SSR specimens can be explained by the increased volume fractions of their GP zones that appear during the natural ageing of these specimens. The volume fraction of GP zones of unstrained Al-Zn-Mg alloys subjected to natural ageing is reported about 2.1% [33]. These results are considerably smaller than those in this work for the SPD processed AA7005. The appearance of a greater volume fraction of GP zones during natural ageing of Al–Zn–Mg alloys after SPD has also been reported in previous work [43], and it can be explained by the increase of diffusion rate of the alloying elements as a result of the imposition of SPD [10,24].

5 Conclusions

- (1) Grain refinement of the alloy through the imposition of SPD is not dependent on the applied pre-deformation heat treatments. For instance, the grain sizes of both artificially aged material and solution treated material equally decrease to about 1 μm after imposition of an equivalent plastic strain about 3 at room temperature.
- (2) The solution treatment, the immediate imposition of SPD combined with the following exposure to several months of natural ageing are excellent procedures for the strengthening of AA7005. As an illustration, the alloy can be strengthened to about 400 MPa, which is one-third greater than the strength of the alloy after the usual T6 treatment.
- (3) The superlative strengthening of the alloy through the mentioned procedure occurs due to a

considerable refinement of grains and an extensive increase of dislocation density through SPD as well as a significant increase of volume fraction of GP zones appeared during subsequent natural ageing of the SPDed alloy.

Acknowledgments

The authors wish to thank the research board of Ferdowsi University of Mashhad (FUM) for the financial support and the provision of research facilities used in this work through grant No. 3/41681. The authors also wish to thank Prof. H. MIYAMOTO and Dr M. ASANO from Doshisha University, Japan for their collaborations in SEM-EBSD experiments.

References

- [1] MALONEY S K, HONO K, POLMEAR I J, RINGER S P. The chemistry of precipitates in an aged Al-2.1Zn-1.7Mg at.% alloy [J]. Scripta Materialia, 1999, 41: 1031-1038.
- [2] NICOLAS M, DESCHAMPS A. Characterisation and modelling of precipitate evolution in an Al–Zn–Mg alloy during non-isothermal heat treatments [J]. Acta Materialia, 2003, 51: 6077–6094.
- [3] RINGER S P, HONO K. Microstructural evolution and age hardening in aluminium alloys: Atom probe field-ion microscopy and transmission electron, microscopy studies [J]. Materials Characterization, 2000, 44: 101–131.
- [4] BERG L K, GJONNES J, HANSEN V, LI X Z, KNUTSON-WEDEL M, WATERLOO G, SCHRYVERS D, WALLENBRG L R. GP-zones in Al-Zn-Mg alloys and their role in artificial ageing [J]. Acta Materialia, 2001, 49: 3443-3451.
- [5] LIU J Z, HU R, ZHENG J L, ZHANG Y D, DING Z G, LIU W, ZHU Y T, SHA G. Formation of solute nanostructures in an Al–Zn–Mg alloy during long-term natural aging [J]. Journal of Alloys and Compounds, 2020, 821: 153572.
- [6] KHALFALLAH A, RAHO A A, AMZERT S, DJEMLI A. Precipitation kinetics of GP zones, metastable η' phase and equilibrium η phase in Al-5.46wt.%Zn-1.67wt.%Mg alloy [J]. Transactions of Nonferrous Metals Society of China, 2019, 29: 233–241.
- [7] SHA G, CEREZO A. Early-stage precipitation in Al–Zn–Mg–Cu alloy (7050) [J]. Acta Materialia, 2004, 52: 4503–4516.
- [8] CHINH N Q, GUBICZA J, CZEPPE T, LENDVAI J, XU C, VALIEV R Z, LANGDON T G. Developing a strategy for the processing of age-hardenable alloys by ECAP at room temperature [J]. Materials Science and Engineering A, 2009, 516: 248–252.
- [9] SAKAI T, BELYAKOV A, KAIBYSHEV R, MIURA H, JONAS J J. Dynamic and post-dynamic recrystallization under hot, cold and severe plastic deformation conditions [J].

- Progress in Materials Science, 2014, 60: 130-207.
- [10] ESTRIN Y, VINOGRADOV A. Extreme grain refinement by severe plastic deformation: A wealth of challenging science [J]. Acta Materialia, 2013, 6: 782–817.
- [11] WANG M L, JIN P P, WANG J H, HAN L I. Hot deformation behavior of as-quenched 7005 aluminum alloy [J]. Transactions of Nonferrous Metals Society of China, 2014, 24: 2796–2804.
- [12] ZHANG S, HU W, BERGHAMMER R, GOTTSTEIN G. Microstructure evolution and deformation behavior of ultrafine-grained Al–Zn–Mg alloys with fine η' precipitates [J]. Acta Materialia, 2010, 58: 6695–6705.
- [13] GUBICZA J, SCHILLER I, CHINH N Q, ILLY J, HORITA Z, LANGDON T G. The effect of severe plastic deformation on precipitation in supersaturated Al–Zn–Mg alloys [J]. Materials Science and Engineering A, 2007, 460–461: 77–85.
- [14] GOPALA KRISHNA K, SIVAPRASAD K, VENKATESWARLU K, HARI KUMAR K C. Microstructural evolution and aging behavior of cryorolled Al-4Zn-2Mg alloy [J]. Materials Science and Engineering A, 2012, 535: 129-135.
- [15] MA K, WEN H, HU T, TOPPING T D, ISHEIM D, SEIDMAN D N, LAVERNIA E J, SCHOENUNG J M. Mechanical behavior and strengthening mechanisms in ultrafine grain precipitation-strengthened aluminum alloy [J]. Acta Materialia, 2014, 62: 141–155.
- [16] ZANGIABADI A, KAZEMINEZHAD M. Development of a novel severe plastic deformation method for tubular materials: Tube Channel Pressing (TCP) [J]. Materials Science and Engineering A, 2011, 528: 5066-5072.
- [17] CHAKRAVARTY S, SIKDAR K, SINGH S S, ROY D, KOCH C C. Grain size stabilization and strengthening of cryomilled nanostructured Cu12at.%Al alloy [J]. Journal of Alloys and Compounds, 2017, 716: 197–203.
- [18] VIMAL G, MANI K P, BIJU P R, JOSEPH C, UNNIKRISHNAN N V, ITTYACHEN M A. Influences of annealing temperature and doping concentration on microstructural and optical properties of CeO₂:Sm³⁺ nanocrystals [J]. Acta Metallurgica Sinica, 2015, 28: 758–765.
- [19] FARSHIDI M H, KAZEMINEZHAD M, MIYAMOTO H. Microstructure and mechanical properties of an Al-Mg-Si tube processed by severe plastic deformation and subsequent annealing [J]. Materials Science and Engineering A, 2015, 640: 42-50.
- [20] FERRAGUT R, SOMOZA A, TOLLEY A. Microstructrual evolution of 7012 alloy during the early stages of artificial ageing [J]. Acta Materialia, 1999, 47: 4355–4364.
- [21] FERRAGUT R, SOMOZA A, TOLLEY A, TORRIJANI I. Precipitation kinetics in Al–Zn–Mg commercial alloys [J]. Journal of Materials Processing Technology, 2003, 141: 35–40.
- [22] HUANG W, LIU Z, LIN M, ZHOU X, ZHAO X, NING A, ZENG S. Reprecipitation behavior in Al–Cu binary alloy after severe plastic deformation-induced dissolution of θ ' particles [J]. Materials Science and Engineering A, 2012, 546: 26–33.

- [23] GUTIERREZ-URRUTIA I, MUNOZ-MORRIS M A, MORRIS D G. Recovery of deformation substructure and coarsening of particles on annealing severely plastically deformed Al-Mg-Si alloy and analysis of strengthening mechanisms [J]. Journal of Materials Research, 2006, 21: 329-342.
- [24] SABIROV I, MURASHKIN M Y, VALIEV R Z. Nanostructured aluminium alloys produced by severe plastic deformation: New horizons in development [J]. Materials Science and Engineering A, 2013, 560: 1–24.
- [25] XU Cu, FURUKAWA M, HORITA Z, LANGDON T G. Influence of ECAP on precipitate distributions in a spray-cast aluminum alloy [J]. Acta Materialia, 2005, 53: 749–758.
- [26] KIM H W, KAN S B, TSUJI N, MNAMINO Y. Elongation increase in ultra-fine grained Al–Fe–Si alloy sheets [J]. Acta Materialia, 2005, 53: 1737–1749.
- [27] KAPOOR R, SARKAR A, YOGI R, SHEKHAWAT S K, SAMAJDAR I, CHAKRAVARTTY J K. Softening of Al during multi-axial forging in a channel die [J]. Materials Science and Engineering A, 2013, 560: 404–412.
- [28] GURRUTXAGA-LERMA B, BALINT D S, DINI D, SUTTON A P. The mechanisms governing the activation of dislocation sources in aluminum at different strain rates [J]. Journal of the Mechanics and Physics of Solids, 2015, 84: 273–292.
- [29] SUZUKI H. Segregation of solute atoms to stacking faults [J]. Journal of the Physical Society of Japan, 1962, 17: 322–325.
- [30] PATINET S, PROVILLE L. Dislocations pinning by substitutional impurities in anatomic-scale model for the Al(Mg) solid solutions [J]. Philosophical Magazine, Part A: Materials Science, 2011, 91: 1581–1606.
- [31] HORVATH G, CHINH N Q, GUBICZA J, LENDVAI J. Plastic instabilities and dislocation densities during plastic deformation in Al-Mg alloys [J]. Materials Science and Engineering A, 2007, 445-446: 186-192.
- [32] DIXIT M, MISHRA R S, SANKARAN K K. Structure–property correlations in Al 7050 and Al 7055 high-strength aluminum alloys [J]. Materials Science and Engineering A,

- 2008, 478: 163-172.
- [33] NICOLAS M, DESCHAMPS A. Precipitate microstructures and resulting properties of Al–Zn–Mg metal inert gas-weld heat-affected zones [J]. Metallurgical and Materials Transactions A, 2004, 35: 1437–1448.
- [34] FARSHIDI M H, RIFAI M, MIYAMOTO H. Microstructure evolution of a recycled Al–Fe–Si–Cu alloy processed by tube channel pressing [J]. International Journal of Minerals, Metallurgy and Materials, 2018, 25: 1166–1172.
- [35] URRUTIA I G, MORRIS M A M, MORRIS D G. Contribution of microstructural parameters to strengthening in an ultrafine-grained Al–7%Si alloy processed by severe deformation [J]. Acta Materialia, 2007, 55: 1319–1330.
- [36] XIAO Q F, HUANG J W, JIANG Y G, JIANG F Q, WU Y F, XU G F. Effects of minor Sc and Zr additions on mechanical properties and microstructure evolution of Al–Zn–Mg–Cu alloys [J]. Transactions of Nonferrous Metals Society of China, 2020, 30: 1429–1438.
- [37] ROBSON J D. A new model for prediction of dispersoid precipitation in aluminium alloys containing zirconium and scandium [J]. Acta Materialia, 2004, 52: 1409–1421.
- [38] DUAN Y, TANG L, XU G, DENG Y, YIN Z. Microstructure and mechanical properties of 7005 aluminum alloy processed by room temperature ECAP and subsequent annealing [J]. Journal of Alloys and Compounds, 2016, 664: 518–529.
- [39] GLADMAN T. Precipitation hardening in metals [J]. Materials Science and Technology, 1999, 15: 30–36.
- [40] FAN H, NGAN A H W, GAN K, EL-AWADY J L. Origin of double-peak precipitation hardening in metallic alloys [J]. International Journal of Plasticity, 2018, 111: 152–167.
- [41] ESTRIN Y. Unified constitutive laws of plastic deformation [M]//Dislocation density related constitutive modeling. Cambridge, Massachusetts: Academic Press, 1996: 69–106.
- [42] TIRYAKIOGLU M. On the relationship between Vickers hardness and yield stress in Al–Zn–Mg–Cu Alloys [J]. Materials Science and Engineering A, 2015, 633: 17–19.
- [43] HU T, MA K, TOPPING T D, SCHOENUNG J M, LAVERNIA E J. Precipitation phenomena in an ultrafine-grained Al alloy [J]. Acta Materialia, 2013, 61: 2163–2178.

大塑性变形和时效处理强化 7005 铝合金

R. BAKHSHI, M. H. FARSHIDI, S. A. SAJJADI

Department of Materials Science and Metallurgical Engineering, Ferdowsi University of Mashhad, Azadi Square, Mashhad, Iran

摘 要:由于7xxx 铝合金在冷变形状态下的可加工性有限,通过大塑性变形和时效处理强化7xxx 铝合金具有挑战性。本研究旨在全面探讨在施加大塑性变形的同时,辅之以两种不同的时效处理工艺:变形前人工时效或变形后自然时效,对7005 铝合金的强化作用。采用 X 射线衍射和扫描电镜研究经上述工艺处理后合金的显微组织演变,并用维氏硬度测试评价合金的强化作用。结果表明,通过施加大塑性变形,辅以变形后自然时效,合金的强化效果最好,其屈服强度提高到400 MPa 以上,比常规 T6 处理后合金的屈服强度提高约1/3。这种高强度主要是由于晶粒细化、位错密度的增加和自然时效过程中析出相体积分数的增加而产生的。结合应用模型推断,自然时效过程中析出相体积分数的增加对合金的强化起决定性作用。

关键词: 大塑性变形; 强度; 析出; 时效处理; 7005 铝合金